LMSC-A665481
29 Dec 1964
Code 9999

PROPELLANT CONTAINMENT UTILIZING SCREEN MESH AND PERFORATED PLATE SURFACES

M. P. Hollister
Research and Development Division
Lockheed Missiles & Space Company
Sunnyvale, California

PROPELLANT CONTAINMENT UTILIZING SCREEN MESH AND PERFORATED PLATE SURFACES

This paper describes a theory and experimental investigation of propellant containment utilizing woven mesh or perforated plate surfaces. A simple theory is presented about which the experimental investigation and data presentation is centered.

Consider a container inclosing a mass of liquid that has a density ρ and surface tension σ against the surrounding gas. See Figure 1. The local acceleration, g, acts in the direction shown. On one side of the container at its extreme top and bottom a distance, h, apart are located holes of radius r. The hole radius is small compared to the local hydrostatic pressure variation so that the liquid-gas interface can be considered spherical with radius R (i.e., hole Bond No. $\frac{\rho g r^2}{\sigma} < 0.1$).

The system contact angle is indicated as θ. Writing the pressure drops across the curved liquid-gas interface at the upper and lower holes in accordance with the Laplace relation:

$$p_o - p_a = \sigma \left(\frac{1}{r_1} + \frac{1}{r_2}\right)_a = \frac{2\sigma}{R_a} \qquad (1)$$

$$p_b - p_o = \sigma \left(\frac{1}{r_1} + \frac{1}{r_2}\right)_b = \frac{2\sigma}{R_b} \qquad (2)$$

the hydrostatic pressure difference between holes is

$$p_b - p_a = \rho g h \qquad (3)$$

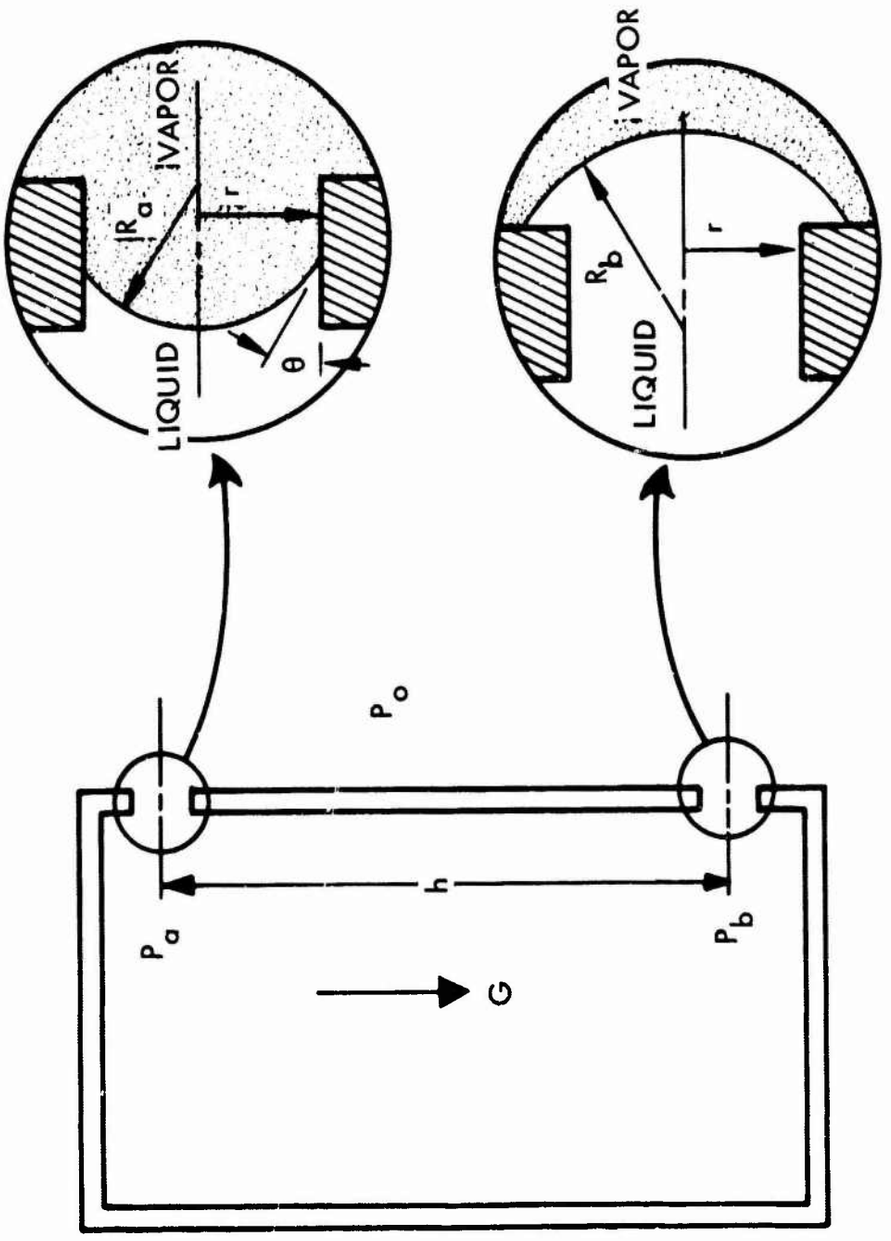

Capillary Supported Containment

FIGURE 1

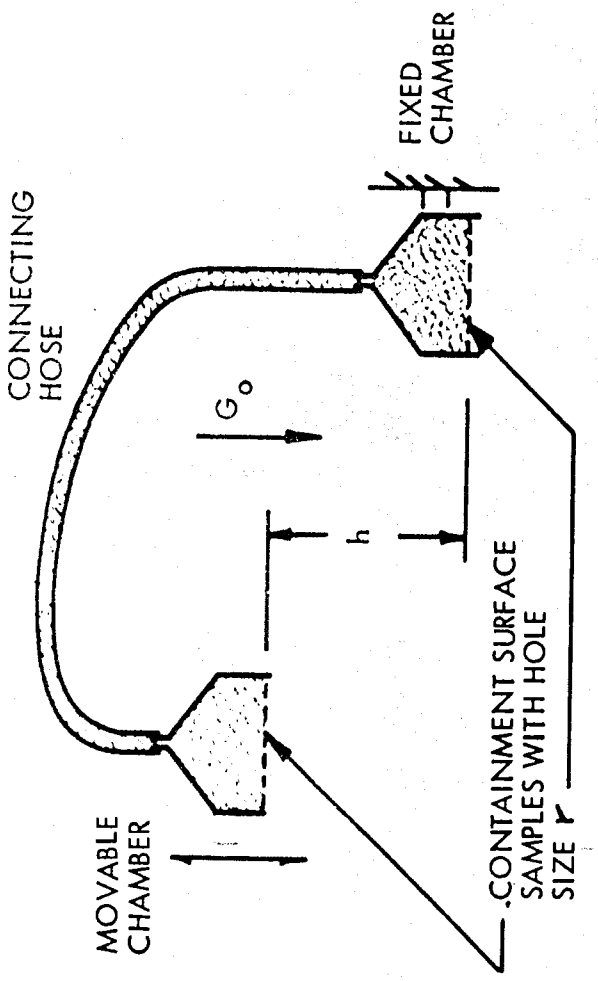

Containment Device Schematic

FIGURE 2

combining (1) (2) and (3) yields

$$\frac{\rho g R_a h}{\sigma} = 2\left(1 + \frac{R_a}{R_b}\right) \qquad (4)$$

From the geometry of the surface at the upper hole

$$r = R_a \cos\theta \qquad (5)$$

Substituting this into (4) yields:

$$\frac{\rho g r h}{\sigma} = 2\left(\cos\theta + \frac{r}{R_b}\right) \qquad (6)$$

The development of an analytical relation beyond this point is dependent on more explicit knowledge of the influence of hole geometry, contact angle, and contact angle hysteresis on the shape and size of the liquid gas interface in the containment surface holes. Rather than attempt this it was decided to group all the known parameters on the left hand side of the equation as was done in relation 6 leaving those aspects about which accurate assumptions could not be made to the right hand side as a non-dimensional constant for the particular system.

Thus we may write:

$$\frac{g r h}{\sigma/\rho} = \underline{\Phi} \qquad (7)$$

where $\underline{\Phi} = \varphi$(contact angle, contact angle hysteresis, containment surface geometry).

A theoretical upper limit for the value of $\underline{\Phi}$ is 4 since this represents one full bubble pressure based on hole radius at the top and one full drop pressure at the bottom based on hole radius. This amounts to an inversion of wetting and is of course difficult to obtain in a practical situation. In this line of thinking for a really good wetting combination ($\theta \approx 0$) a $\underline{\Phi}$ value of 2 would indicate one "bubble pressure" based on hole radius with no aid to containment furnished by the "lower" holes.

During May 1963 a limited experimental investigation into the validity of relation 7 and into the influence of wetting characteristics and hole geometry on the value of $\underline{\Phi}$ was undertaken at LMSC. A simple apparatus was fabricated to set up a hydrostatic pressure difference between two containment surfaces by virtue of a height h at 1 g_o acceleration. This is depicted schematically in Figure 2.

Basically the device consisted of two chambers connected by a flexible hose. A sample of the containment surface to be tested was placed in each chamber in a horizontal position and the apparatus above the screens filled with the liquid to be tested. The movable chamber was then raised relative to the fixed chamber to that value where gas in the form of bubbles was observed passing through the upper containment surface indicating that the containment surface was no longer able to provide a static balance against the hydrostatic pressure difference. In this manner a number of containment surface geometries were tested with distilled water, methyl alcohol, UDMH and IRFNA as the contained liquids. Together with the materials composing the containment surface a limited range of wetting characteristics was obtained. Listed below are the surface samples tested.

TABLE I

Sample No.	Hole Size (cm)	Configuration	Material
1	.004	Screen Mesh	Stainless Steel
2	.0075	Screen Mesh	Stainless Steel
3	.0069	Screen Mesh	Stainless Steel
4	.0081	Screen Mesh	Stainless Steel
5	.030	Screen Mesh	Stainless Steel
6	.016	Screen Mesh	Teflon
7	.023	Screen Mesh	Teflon
8	.017	Perforated Plate	Teflon
9	.022	Perforated Plate	Teflon
10	.031	Perforated Plate	Teflon
11	.016	Perforated Plate	Aluminum
12	.027	Perforated Plate	Aluminum

The results of the tests were displayed on plots of containment surface holes size r vs h and compared with constant Φ values of 1, 2 and 4 as shown in Figures 3, 4, and 5. From these considerations a Φ value can be obtained to be used in containment system design. The information contained in Figure 5 was used in the design of a propellant containment system currently employed on an Advanced Agena configuration.

The following features of the data presented seem noteworthy. First the trend of the data parallels the theoretical curves. Thus for a particular system the equation $\rho g r h/\sigma = \Phi$ is valid wherein Φ is constant for a particular liquid-solid system and containment surface geometry.

All the data points lie below $\Phi = 4$ line the theoretical upper limit for containment and seem to be grouped about the $\Phi = 2$ line indicating containment capability less than the theoretical maximum. This is of course to be expected since without specific design an inversion of wetting between the upper and lower holes is not possible.

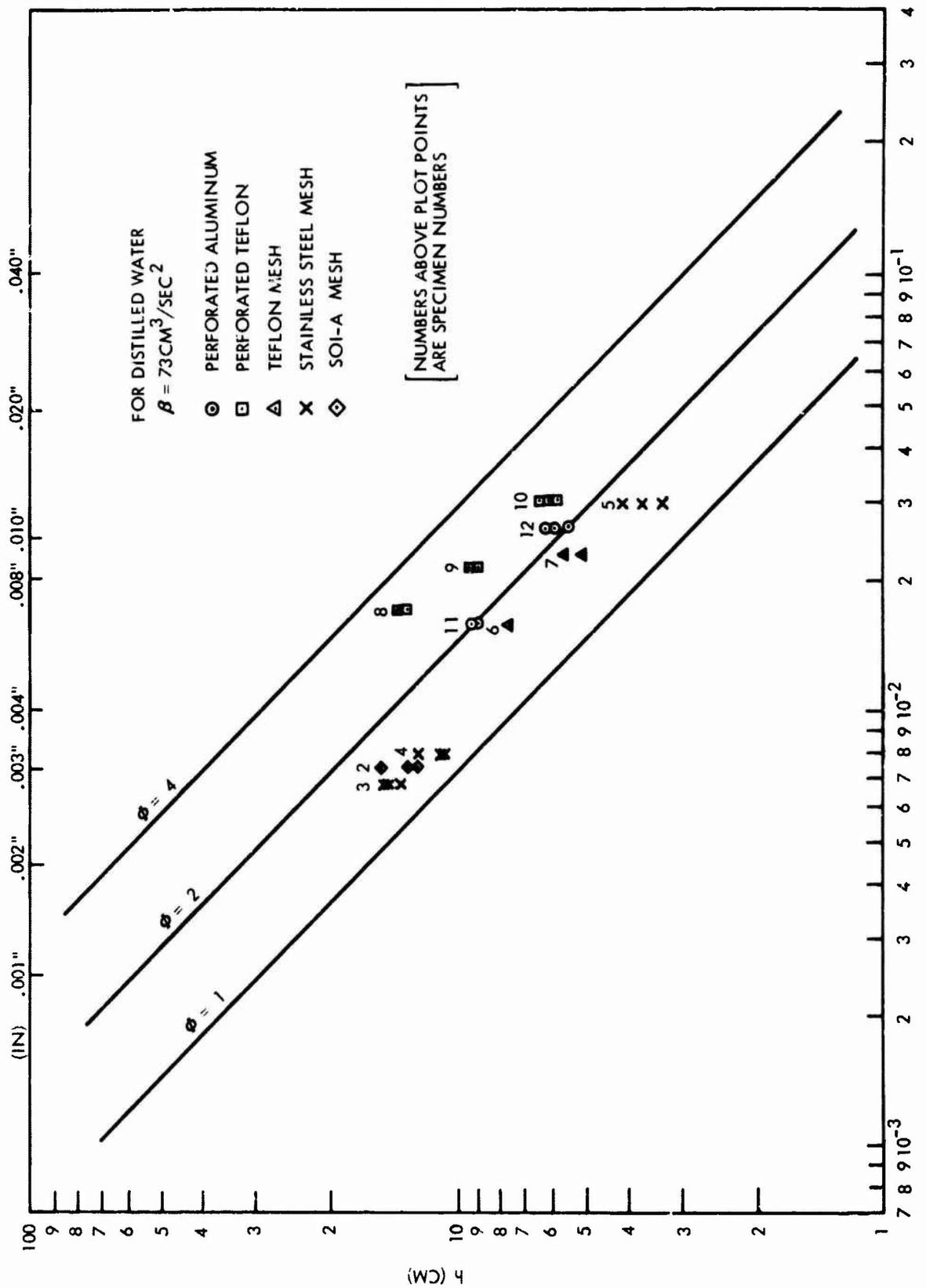
FOR DISTILLED WATER
β = 73CM^3/SEC^2
PERFORATED ALUMINUM
PERFORATED TEFLON
TEFLON MESH
STAINLESS STEEL MESH
SOI-A MESH
[NUMBERS ABOVE PLOT POINTS ARE SPECIMEN NUMBERS]
ϕ = 4
ϕ = 2
ϕ = 1
h (IN) .001" .002" .003" .004" .008" .010" .020" .040"
h (CM)
r (CM)

FIGURE 3

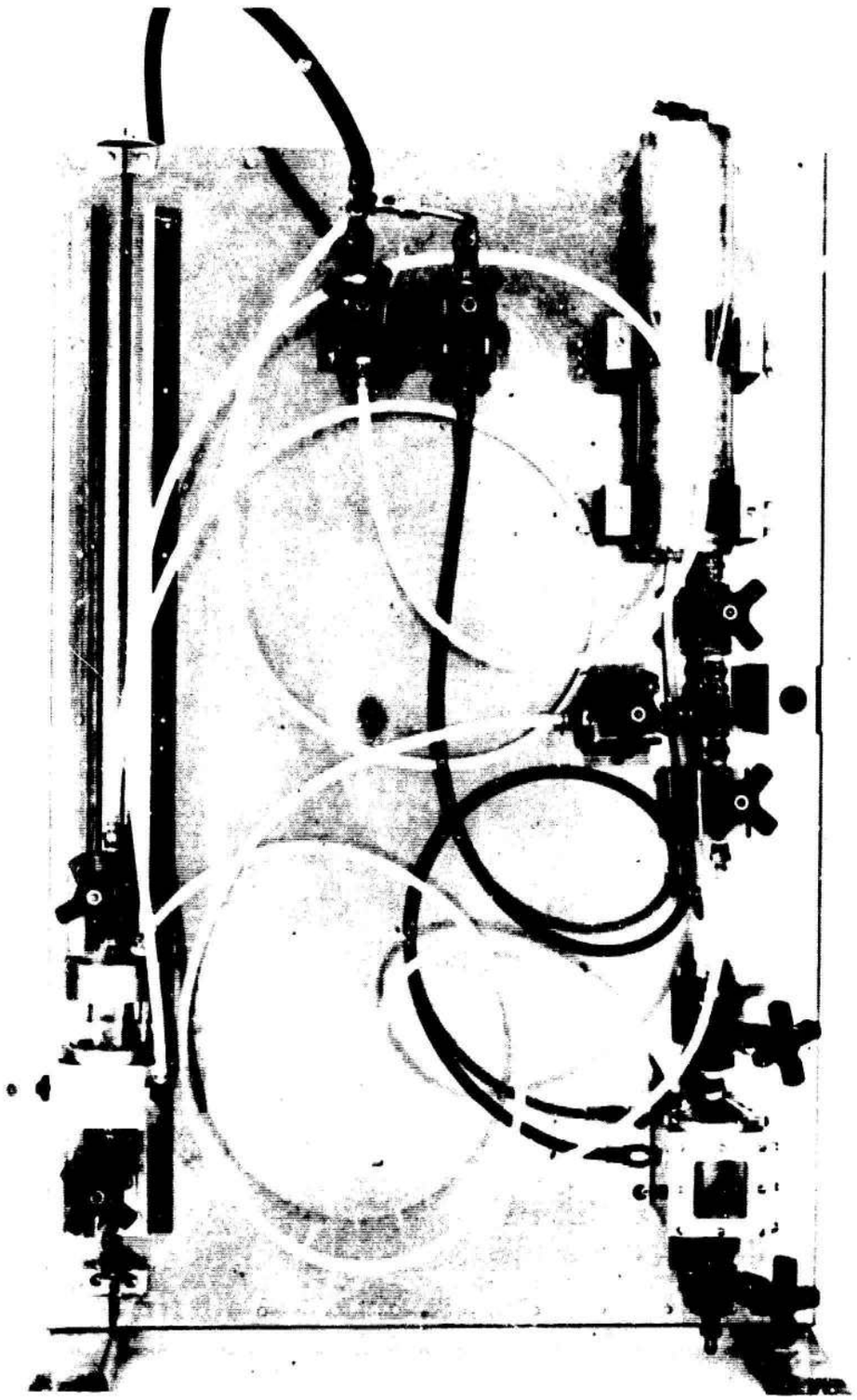

Containment Test Device

FIGURE 3a

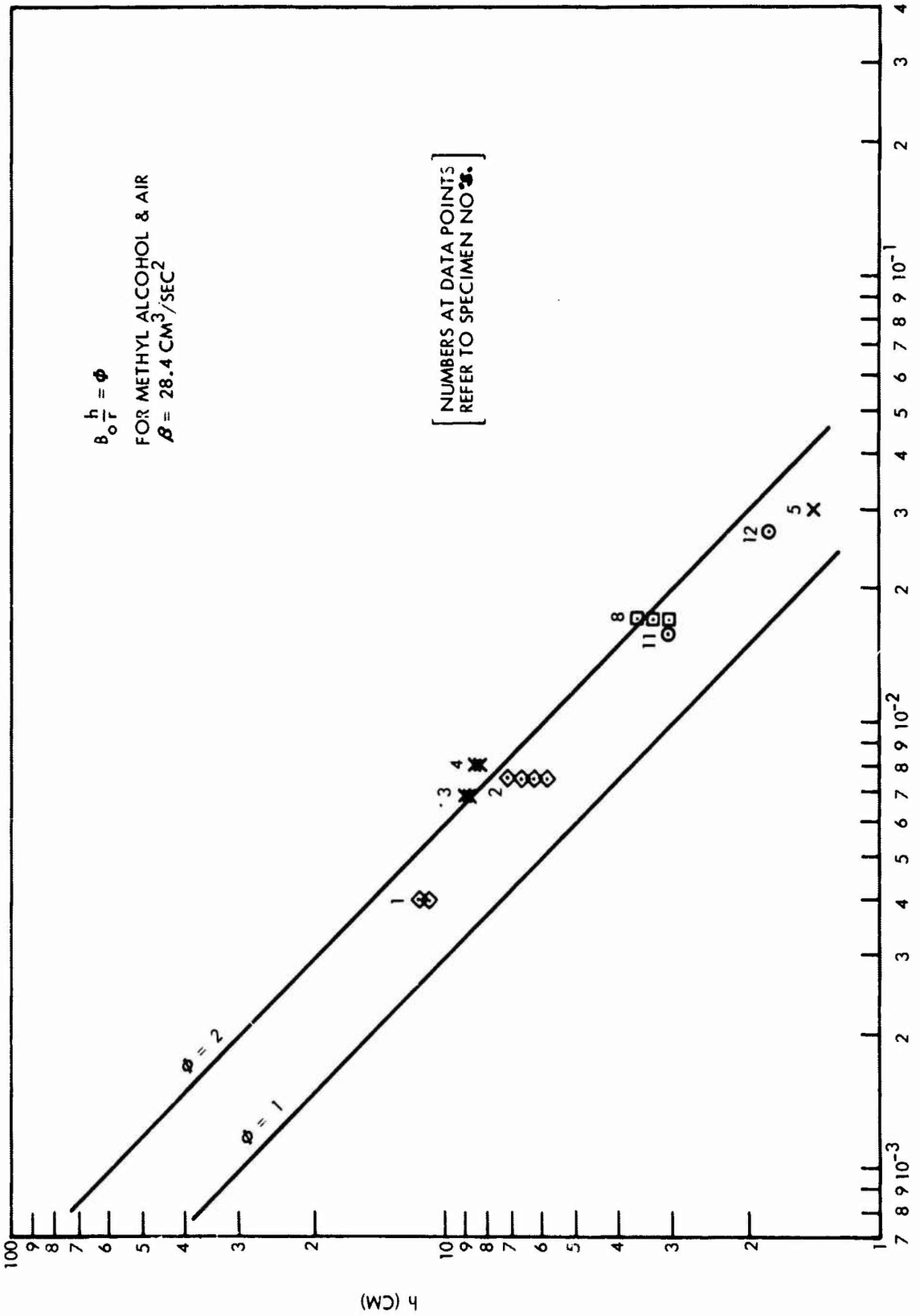
$\beta_o \frac{h}{r} = \phi$
FOR METHYL ALCOHOL & AIR
$\beta = 28.4\ CM^3/SEC^2$
[NUMBERS AT DATA POINTS REFER TO SPECIMEN NO's.]
$\phi = 2$
$\phi = 1$
h (CM)
r (CM)

FIGURE 4

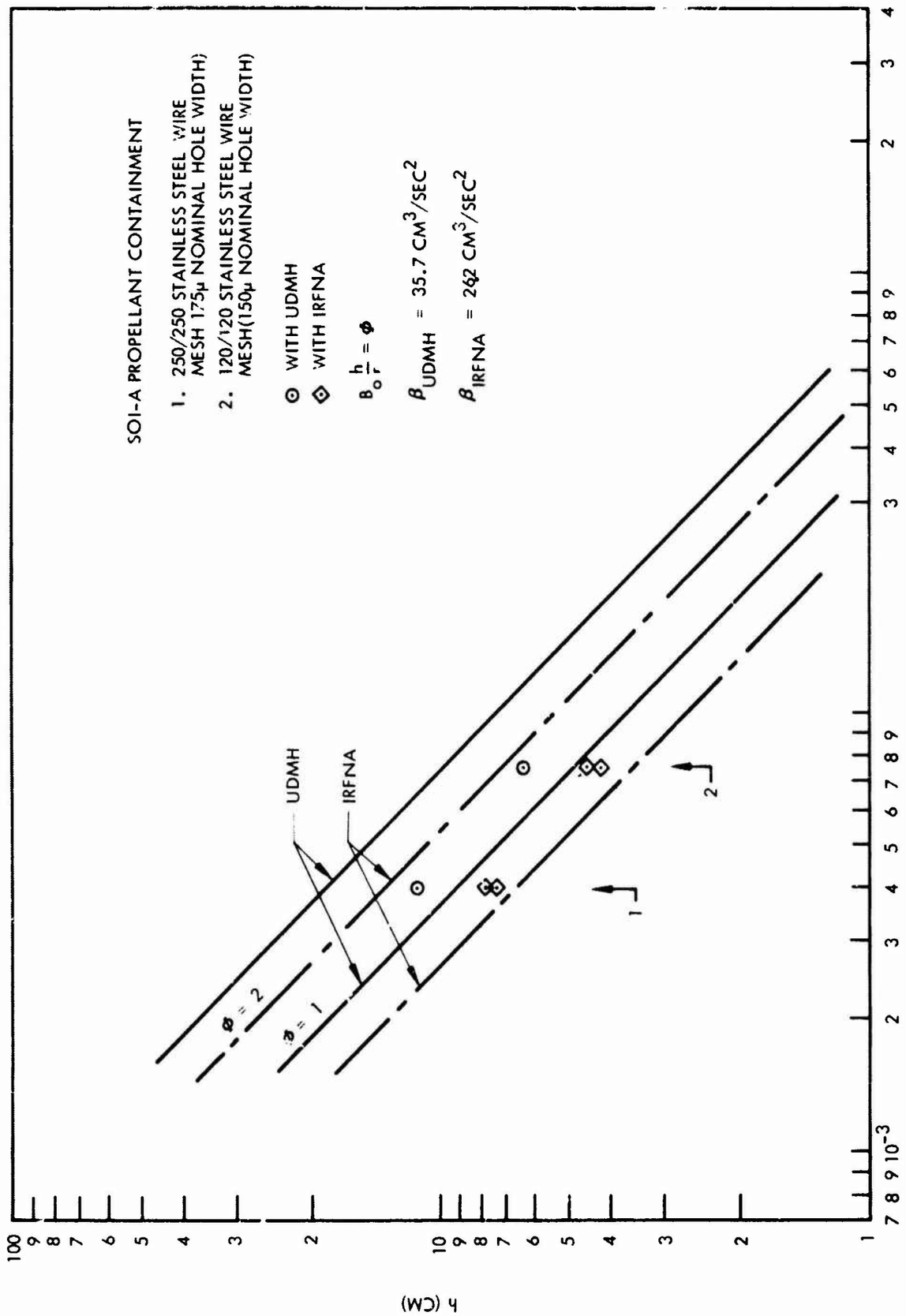
SOI-A PROPELLANT CONTAINMENT
1. 250/250 STAINLESS STEEL WIRE MESH 175μ NOMINAL HOLE WIDTH)
2. 120/120 STAINLESS STEEL WIRE MESH(150μ NOMINAL HOLE WIDTH)
⊙ WITH UDMH
◇ WITH IRFNA
$B_o \frac{h}{r} = \phi$
β_{UDMH} = 35.7 CM^3/SEC^2
β_{IRFNA} = 262 CM^3/SEC^2
UDMH
IRFNA
ϕ = 2
ϕ = 1
1
2
h (CM)
r (CM)

FIGURE 5

The contact angle of water and the containment materials used (aluminum, stainless steel, and teflon) is large (80° - 90°). Thus Figure 3 represents the behavior of poorly wetted systems. For this situation there is an apparent grouping of perforated containment geometry above the wire screen geometry indicating that for liquid-solid combinations that are nearly neutral in wetting characteristics a perforated surface will give better containment. With a good wetting combination such as is represented by the methanol tests (Figure 4) this advantage of perforated over screen mesh geometry is not apparent.

Those points above the $\mathcal{Q}$ = 2 line (perforated teflon) would indicate that some additional containment was obtained due to the formation of and corresponding pressure differential associated with drops of the water in the holes. This is partly confirmed by the observation of individual drops on the low side of the perforated teflon samples during the tests. In all other cases the low or drop side of the containment system appeared to be sufficiently wetted so as to prevent the formation of drops and any increase in containment stability therefrom.

In order to examine a little further the effect of hole geometry and wetting characteristics as noted above an anlysis of bubble protrusion past a rod in two dimensions was performed and is shown in Appendix I. This correction in effect converts from hole radius to an equivalent bubble radius. Based on this analysis correction factors were obtained, applied to the screen mesh data on Figure 3 and replotted in Figure 6.

These corrections bring the performance of the screen mesh or wire grid close to that of the perforated geometry which indicates at least qualitatively that some of the poor containment behavior of screen mesh with relatively neutral wetting liquids is due to the circular rather than rectangular cross sectional geometry of the containment material.

As the curves of Figure I-2 appendix I indicate for low contact angle configurations this effect of cross sectional geometry is not present. The data for methanol plotted on Figure 2 confirm this by the closer grouping of points about the $\mathcal{Q}$ = 2 line.

Figure 3 is a plot of the containment behavior of two particular screen mesh configurations originally proposed for incorporation into the Agena design (samples 1 and 2). Since the containment capability of these particular screen geometries seems to consistancy below the $\mathcal{Q}$ = 2 line in the neighborhood of $\mathcal{Q}$ = 1.5 regardless of the degree of wetting there is an indication that some feature peculiar to these geometries is causing the decrease in capability relative to a standard screen mesh. Since this slight disparity is of no real importance to the ultimate behavior of the vehicle containment system no effort was made to explain it and indicate methods for improving the design in this respect.

Finally since it was not the objective of this program to investigate in a precise manner the functional relationship $\mathcal{Q} = \varphi$ (contact angle, contact angle hysteresis and containment surface geometry), and since the containment surface specimens used incorporated no precise control

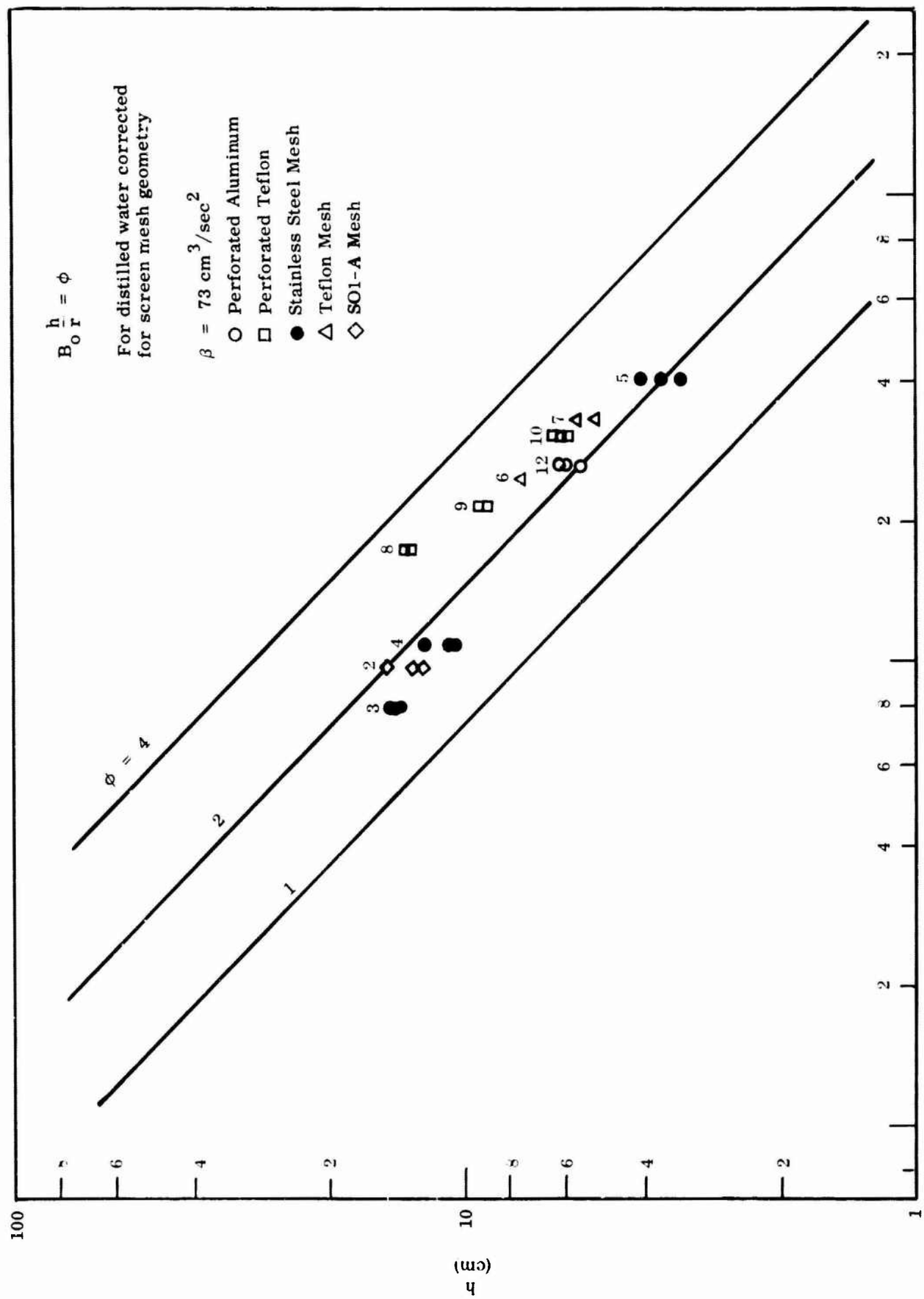
$B_o \frac{h}{r} = \phi$
For distilled water corrected for screen mesh geometry
β = 73 cm^3/sec^2
O Perforated Aluminum
□ Perforated Teflon
● Stainless Steel Mesh
△ Teflon Mesh
◇ SO1-A Mesh
ϕ = 4
2
1
h (cm)
r (cm)
100
10
1
10^{-3}
10^{-2}
10^{-1}

FIGURE 6

of these variables, no further conclusions can be drawn from the data except to note that improvement of containment capability might be obtained by proper design configuration of the containment surface.

Appendix I
BUBBLE PROTRUSION PAST A WETTED ROD GRID

Consider the two-dimensional solid-liquid-gas configuration sketched below. Parallel rods with radius r_1 and separation d are placed in the liquid-gas interface. The contact angle at the solid-liquid-gas junction is θ. The dimension d is small enough to satisfy the assumption of a circular liquid-gas interface curve.

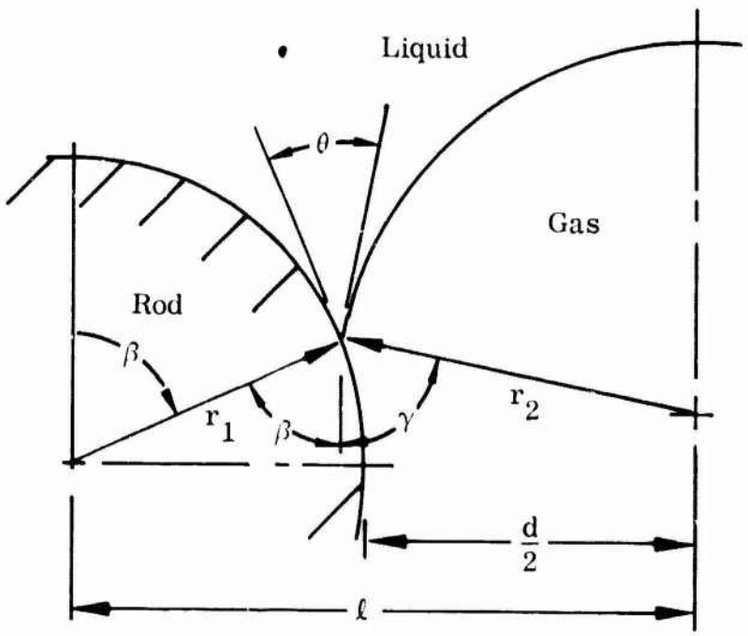

$$\gamma = \pi - (\theta + \beta)$$

$$\ell = r_1 \sin\beta + r_2 \sin\gamma$$

$$= r_1 \sin\beta - r_2 \sin(\theta + \beta)$$

$$\ell = r_1 + \frac{d}{2}$$

Let

$$r_1 = ad \quad ; \quad \ell = kd \quad ; \quad k = \frac{2a + 1}{2}$$

$$kd = ad \sin \beta - r_2 \sin (\theta + \beta)$$

$$r_2 = \frac{ad \sin \beta - kd}{\sin (\theta + \beta)}$$

$$\frac{r_2}{d} = \frac{a \sin \beta - k}{\sin (\theta + \beta)} \tag{I-1}$$

With parameters a and θ find β that gives minimum r_2/d.

$$\frac{d}{d\beta}\left(\frac{r_2}{d}\right) = \frac{a \cos \beta}{\sin (\theta + \beta)} - \frac{a(\sin \beta - k)\cos(\theta + \beta)}{\sin^2 (\theta + \beta)} = 0$$

$$\frac{\cos \beta}{\sin \beta - k} = \cot (\theta + \beta) \tag{I-2}$$

Relation 2 is plotted on Figure I-1 for a = 1, 0.5, and 0.25 and for $\theta = \pi/2$, $\pi/3$, and $\pi/6$. From these curves the curves of Figure I-2 have been generated. Figure I-2 indicates the actual bubble size for a maximum stabilizing pressure differential across the curved liquid-gas interface.

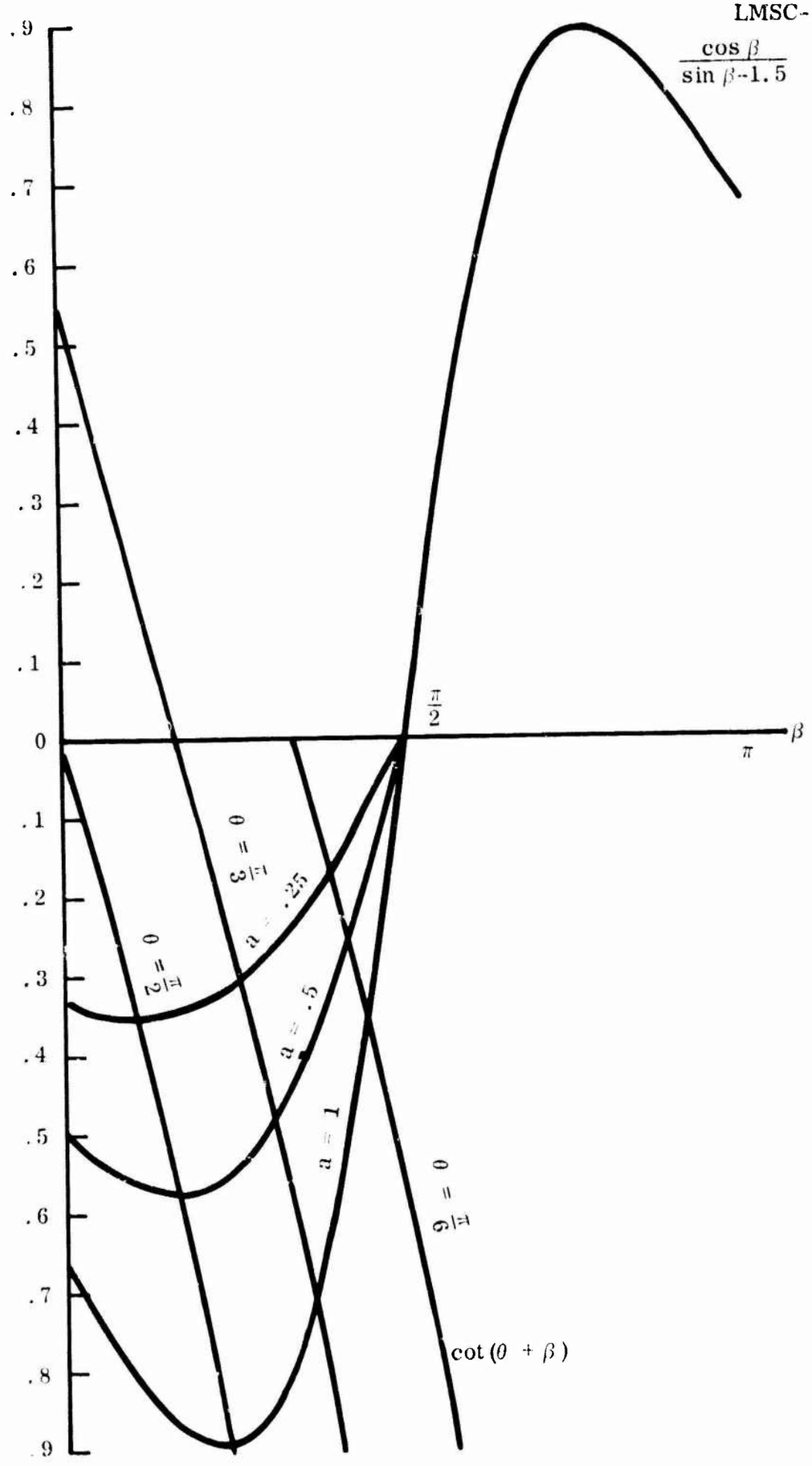

Fig. I-1 Graph of Equation (I-2)

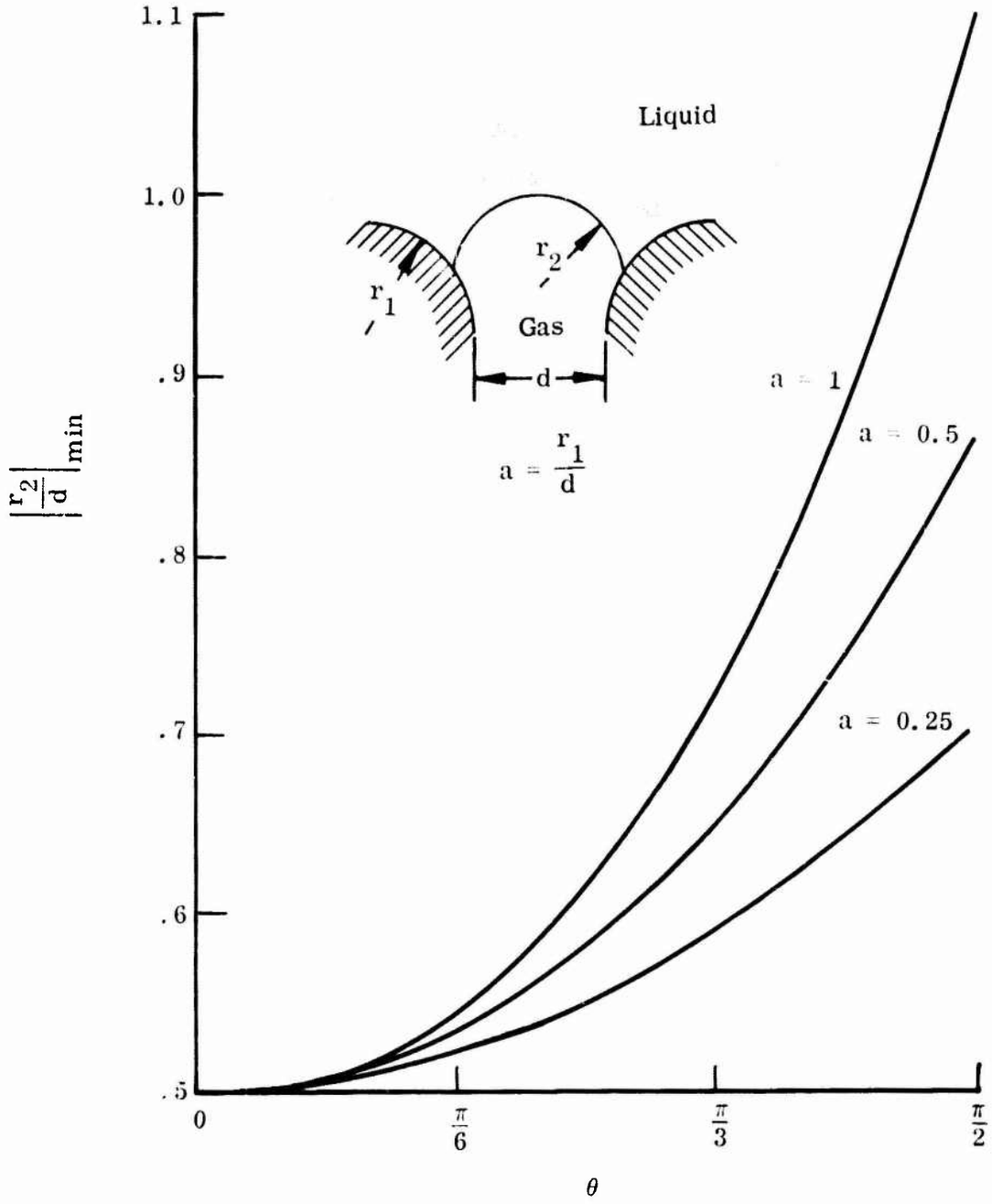

$$r_{hole} = \frac{d}{2} \qquad r_2 = \frac{r_2}{d} \cdot \frac{d}{r_{hole}} \cdot r_{hole}$$

Actual Bubble Radius: $r_2 - 2\left|\frac{r_2}{d}\right| r_{hole}$

Fig. I-2 Bubble Size for Maximum Capillary Pressure